RSC Advances

PAPER

View Article Online
View Journal | View Issue

Cite this: *RSC Adv.*, 2025, **15**, 33531

Dynamic pedal motion and thermal expansion in an ionic co-crystal with 1,2-bis(4-pyridyl) ethylene

Yuchen Zhang,[a] Yijia Jiao,[a] Yan Guo,*[a] Peipei Cen,*[b] Zhenyi Zhang[c] and Xiangyu Liu*[a]

Received 10th July 2025
Accepted 10th September 2025

DOI: 10.1039/d5ra04941e

rsc.li/rsc-advances

An ionic co-crystal material (**Bpe-BPh4**) composed of 1,2-bis(4-pyridyl) ethylene (Bpe) molecules and sodium tetraphenylborate ($NaBPh_4$) is synthesized and isolated. Single crystal X-ray diffraction reveals that the molecular structure of the co-crystal contains a protonated $HBpe^+$ cation and a $[BPh_4]^-$ anion. Interestingly, variable-temperature single crystal X-ray experiments show that the material exhibits temperature-dependent pedal motion with dynamic disorder of the Bpe moiety, leading to thermal expansion (TE) behaviour within the **Bpe-BPh$_4$** molecules, which confers responsiveness to thermal stimuli. A Thermal Expansion Visualizing (TEV) method was employed to further investigate the TE process. This discovery provides valuable guidance for designing advanced materials with tunable thermal properties.

Introduction

The ability to alter and control the properties of solid-state materials remains an important and challenging area of research.[1] Co-crystals have emerged as valuable materials to vary both the chemical and physical properties in multi-component crystalline solids, because these properties can be vastly different when compared to those of the constituent molecules.[2] Changes in these properties, such as reactivity,[3] thermal expansion (TE),[4] and molecular motion,[5] frequently arise by achieving different crystal packing arrangements within the co-crystal that contrast that of the single-component solid. Specifically, TE, the response of a material to temperature change, represents an ongoing and major challenge.[6]

As is known, 1,2-bis(4-pyridyl) ethylene (Bpe) molecules offer several advantages that make them highly promising for a wide range of applications.[7–9] The flexible molecular structure of Bpe allows for adaptation to various environmental conditions,[10] enabling the adjustment of physical and chemical properties to meet diverse needs. In particular, bipyridines include bridging groups (such as azo (N=N) or ethylene (C=C)) that exhibit dynamic pedal motion,[11] and the resulting TE parameters correlate with the tendency of the bridge to bear this type of molecular motion.[12] In this case, with strong chemical stability, Bpe retains consistent performance even after repeated use, making it ideal for long-term applications. Compared to conventional N=N-based systems, the distinctive C=C core and dipyridyl architecture of Bpe offer both economic advantages and enhanced structural functionality, enabling the construction of stable yet flexible one-dimensional assemblies through optimized hydrogen-bonding interactions. Overall, Bpe molecules show great potential across fields such as materials science, electronic devices, and nanotechnology.

In this study, a one-dimensional hydrogen-bonded organic ionic co-crystal, **Bpe-BPh$_4$**, was successfully obtained through a high-yield protonation. The material exhibits unique behaviours arising from disorder and molecular motion within the crystal. Increasing temperature induces molecular dynamics that resemble pedal motion, accompanied by a significant thermal expansion (TE) process. Complementary variable-temperature single-crystal (molecular conformation) and powder (phase behaviour) X-ray analyses reveal these multiscale thermal responses. The underlying molecular dynamic mechanisms have been systematically investigated, providing new insights into structure–property relationships in dynamic crystalline materials.

Experimental section

Synthesis of Bpe-BPh$_4$

A solution of Bpe (0.018 g, 0.1 mmol) in methanol (15 mL) and HCl (0.5 mL) was prepared and stirred for 30 min. $NaBPh_4$ (0.034 g, 0.1 mmol) was added to the solution which was stirred for 3 h at room temperature. After filtration, the filter residue was naturally dried at room temperature to obtain yellow crystals Anal. calcd for $C_{36}H_{31}BN_2$ (502.456): C, 86.05; N, 6.22; H,

[a]*State Key Laboratory of High-Efficiency Utilization of Coal and Green Chemical Engineering, College of Chemistry and Chemical Engineering, School of Civiland Hydraulic Engineering, Ningxia University, Yinchuan 750021, China. E-mail: xiangyuliu432@126.com; gy2020054@163.com*

[b]*College of Public Health, Key Laboratory of Environmental Factors and Chronic Disease Control, Ningxia Medical University, Yinchuan 750004, China. E-mail: 13895400691@163.com*

[c]*Bruker Scientific Instruments (Shanghai) Co., Ltd, China*

5.57%. Found: C, 85.84; N, 6.21; H, 5.54%. ^{1}H NMR (500 MHz, DMSO) δ 8.79 (d, J = 5.6 Hz, 2H), 7.94 (d, J = 5.6 Hz, 2H), 7.84 (s, 1H), 7.18 (t, J = 6.2 Hz, 4H), 6.92 (t, J = 7.3 Hz, 4H), 6.78 (t, J = 7.2 Hz, 2H). ^{13}C NMR (126 MHz, DMSO) δ 164.43, 164.03, 163.64, 163.25, 147.84, 146.93, 136.01, 133.08, 125.80, 125.78, 125.76, 125.74, 123.32, 121.98.

Materials and physical measurements

All chemicals were reagent grade and commercially available. All chemicals were received for direct use without further purification. The phase purity of the bulk or polycrystalline samples were measured by Powder X-ray diffraction (PXRD) measurements executed on a Rigaku RU200 diffractometer at 60 kV and 300 mA, using Cu Kα radiation (λ = 1.5406 Å), with a scan speed of 5° min^{-1} and a step size of 0.02° in 2θ. Thermogravimetric (TG) analysis is carried out on a STA8000 system analyzer under an N_2 atmosphere at a heating rate of 10 °C min^{-1} within the temperature ranging from 30 to 800 °C.

Single crystal X-ray diffraction measurements

Suitable crystal of the ionic co-crystals was selected for X-ray measurements. The crystal structure was collected with a Bruker SMART APEX-CCD-based diffractometer using graphite mono chromated Mo Kα radiation (λ = 0.71073 Å) at room temperature. Subsequently, crystal data were collected at 140–320 K using Cu Kα radiation (λ = 1.54178 Å). The structure of **Bpe-BPh$_4$** was solved with the *SHELXT* structure solution program using intrinsic phasing, and refined by full-matrix least-squares on F^2 using *SHELXL*, interfaced through *OLEX2*. All non-hydrogen atoms were refined with anisotropic displacement parameters, while all hydrogen atoms have been placed on idealized positions using the program *OLEX2*. Basic information pertaining to the crystal parameters and structure refinement are summarized in Table S1.

Results and discussions

Single-crystal X-ray diffraction at 290 K reveals that **Bpe-BPh$_4$** crystallizes in the monoclinic $P2_1/n$ space group, featuring dynamically disordered HBpe$^+$ cations and ordered [BPh$_4$]$^-$ anions (Fig. 1a). As shown in Fig. S1 and S2, the protonated HBpe$^+$ cations are interactively sustained by N–H···N hydrogen bonds to form a one-dimensional chain in space. The N–H···N hydrogen bonds have a consistent length of 2.686 Å. These hydrogen bonds are formed by a protonated nitrogen atom (N2) of the pyridine group in a HBpe$^+$ molecule, which serves as the hydrogen bond donor, while an unprotonated nitrogen atom (N1A) in another neighboring HBpe$^+$ molecule acts as the acceptor. This interaction plays a crucial role in stabilizing the one-dimensional chain structure and significantly contributes to the overall molecular arrangement and structural integrity. The [BPh$_4$]$^-$ anions occupy the space between adduct cations, serving as counter anions. Interestingly, each HBpe$^+$ is disordered over two sites (site occupancies: 0.67 and 0.33) with the dominate conformation being A, and the other being conformation B. These two conformations are related to each other by an approximate 2-fold rotation along the longest axis of the molecule. Note that conformations A and B can be transformed into each other by pedal motion in the molecule.

In the course of the pedal motion, both pyridine rings in HBpe$^+$ move like bicycle pedals. In conformation A, the two rings are parallel to each other like the two pedals in a bicycle.[11] During the pedal motion, the orientations of both pyridine rings change slightly relative to the crystal lattice, and the two rings remain parallel to each other. Nevertheless, the orientation of the C=C bond alters significantly. The dihedral angle between the two rings increases to almost 90° at the transition state. Ultimately, the C=C bond rotates 180°, leading to the transformation of the entire HBpe$^+$ moiety to the other conformation B. In this regard, the two pyridine rings can be identified as rotating simultaneously in opposite directions, coupled with the overall molecular rotation. The coexistence of pedal motion and conformational interconversion in the crystal gives rise to the randomly distributed two alternating conformations observed as disorder in the structure. In principle, a dynamic equilibrium can be established during the process of the conformational interconversion, which would contribute to a gradual change in the populations of the conformations with varying temperature according to the Boltzmann distribution, thus resulting in dynamic disorder.[11] Conversely, the populations would remain constant at different temperatures if the disorder is static and the two conformations do not interconvert. Accordingly, it is crucial to analyse the temperature dependence of the populations in different conformations for the determination of the conformational interconversion in the structure.[13]

The purity of **Bpe-BPh$_4$** sample was analyzed by powder XRD with the 2θ angle ranging from 5° to 50°. As shown in Fig. S4, the red line refers to the experimentally obtained XRD curve, while the black line presents the simulated curve from crystal data. The generally consistent diffraction curves between experimental and simulated spectra indicates the purity and structural homogeneity of the samples.

In order to analyze the thermostability for **Bpe-BPh$_4$**, the powder XRD of **Bpe-BPh$_4$** was collected from 25 to 125 °C, as depicted in Fig. 2a. No significant changes are observed among tested temperatures. Also, the thermostability of **Bpe-BPh$_4$** was measured in the range of 30–750 °C under N_2 atmosphere. As displayed in Fig. 2b, the observed rise in weight percent between 30-150 °C is due to the measuring instrument failing to

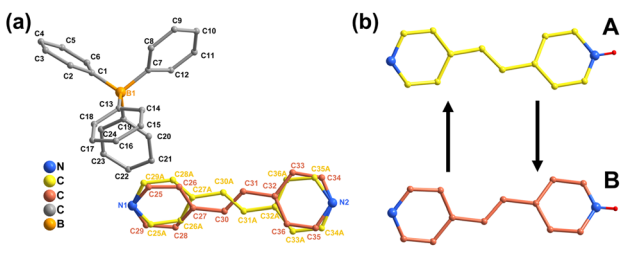

Fig. 1 (a) Crystal structures of the cation of **Bpe-BPh$_4$**. The hydrogen atoms on the carbon are omitted for clarity. (b) The transition motion of **Bpe-BPh$_4$**, conformation A to conformation B.

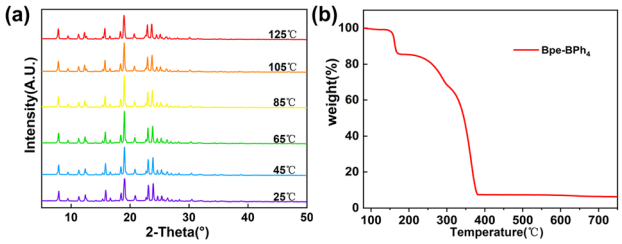

Fig. 2 (a) Variable-temperature powder XRD of **Bpe-BPh$_4$**. (b) TG curve of **Bpe-BPh$_4$**.

enable the sample to undergo proper equilibration before the experiment started. The TG curve suggests that **Bpe-BPh$_4$** is thermally stable up to 150 °C, which is corresponds to the PXRD results. After 150 °C, the sample occurs weight loss. At 150–160 °C, the structure undergoes partial collapse. Subsequently, the structure completely collapses above 350 °C. Such two-step thermal decomposition of **Bpe-BPh$_4$** is inconsistent with the one step decomposition behaviour of both raw materials Bpe and $NaBPh_4$ (Fig. S5 and S6).

In order to analyze whether the disorder state is static or dynamic, an *in situ* variable-temperature single-crystal X-ray diffraction (SCXRD) study was performed on the **Bpe-BPh$_4$** crystal sample (Table 1), where conformation A is the major form, while conformation B is the minor one. The crystallographic data were collected at seven different temperatures (140, 170, 200, 230, 260, 290, and 320 K). A comparison of the structures at varying temperatures unveils that the $[BPh_4]^-$ segments are ordered from 140–320 K, whereas the $HBpe^+$ molecules are always disordered. As a result, the disorder of the $HBpe^+$ molecule is indeed dynamic after collecting and refining the additional SCXRD data. It is demonstrated that pedal motion occurred in **Bpe-BPh$_4$** as there were changes in the occupancies of the disordered conformations throughout the heating. The disorder of $HBpe^+$ groups is enhanced as the temperature gradually increases from 140 K to 320 K (Fig. S3). It is found that the thermally dynamic variation not only modulates the pedal motion of $HBpe^+$ molecules, but also manipulates the site occupancy factors (SOFs) of the molecules, which change significantly from 50.2/49.8 at 140 K to 72.3/27.7 at 320 K. Accordingly, the variable-temperature SCXRD study suggests the molecular pedal motion involving $HBpe^+$ groups in **Bpe-BPh$_4$**.[14]

Table 1 Pedal motion in crystals of **Bpe-BPh$_4$** indicated by changes in the occupancies of the C=C crystallographic sites, respectively

Temperature/K	(Major/minor)
140	50.2/49.8
170	55.5/44.5
200	60.1/39.9
230	63.6/36.4
260	67.2/32.8
290	69.6/30.4
320	72.3/27.7

It is reported that fine-tunings of molecular level structure would be transduced into the unit cell of single crystals, due to the uniaxially structural stackings and intermolecular interactions.[15] The changes in unit cell parameters occur, while the crystal system and space group are retained. When heating in the range of 140–320 K, the *a*, *b* and *c* axes, and volume are all prominently expanded (Fig. 3 and Table S2), which corresponding to the previously reported molecular pedal motion upon temperature rising,[16] further supporting the rotationally structural transformation of the molecules. In the unit cell of **Bpe-BPh$_4$**, the *a*, *b*, and *c* axes increase by 1.4%, 1.5%, and 1.3%, respectively, while the volume of each molecule alters from 2740.1 to 2844.3 Å^3 in the range of 140–320 K with a growth rate of 3.8%, which is often referred to as TE.[17–19]

Based on the formalism for the infinitesimal temperature limit introduced by Paufler and Weber, the TEV[20] software was used to calculate the components of the thermal expansion tensor α_{ij}. For the definition of the second-rank tensor in the TEV program, the following orthogonal coordinate system was used: *e*3 is parallel to the *c*-axis, *e*2 is parallel to *b**, and *e*1 = *e*2 × *e*3. The resulting symmetrical tensor has six independent components (α_{11}, α_{22}, α_{33}, α_{12}, α_{13}, α_{23}); due to the symmetry constraints of the monoclinic crystal system (with the unique axis *b*), the components α_{12} and α_{23} are zero. After transformation to the principal axes, the tensor can be further simplified and described by only three independent components (α_1, α_2, α_3). The temperature dependence of the thermal expansion eigenvalues and tensor is compiled in Tables 2 and 3. Although each individual expansion coefficient shows only subtle changes with temperature, differences in values along different directions are still observed, which makes the thermal expansion of **Bpe-BPh$_4$** anisotropic. The tensor and its anisotropy are represented as a surface in three-dimensional space, as shown in Fig. 4. This variation along different axes demonstrates the anisotropic nature of thermal expansion in **Bpe-BPh$_4$**, consistent with the crystal symmetry and exhibiting distinct thermal expansion behaviours along different directions. This study demonstrates that a hydrogen-bonded 1D supramolecular architecture exhibits unique thermoresponsive behaviour, serving as both a model system for dynamic materials and a design platform for multidimensional functional assemblies.

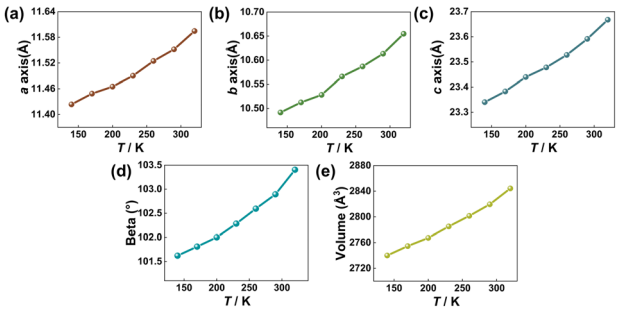

Fig. 3 Unit-cell parameters as a function of temperature for **Bpe-BPh$_4$**.

Table 2 Temperature dependence of the tensor of the thermal expansion coefficients of **Bpe-BPh$_4$**

Temp.[K]	α_{11}	α_{22}	α_{33}	α_{12}	α_{13}	α_{23}
140	1.08×10^{-4}	9.87×10^{-5}	2.26×10^{-5}	0	-9.64×10^{-5}	0
170	2.04×10^{-5}	4.97×10^{-5}	8.18×10^{-5}	0	-4.03×10^{-5}	0
200	2.97×10^{-5}	8.27×10^{-5}	6.81×10^{-5}	0	-6.91×10^{-5}	0
230	5.26×10^{-5}	9.92×10^{-5}	5.67×10^{-5}	0	-9.40×10^{-5}	0
260	5.35×10^{-5}	7.87×10^{-5}	7.61×10^{-5}	0	-9.03×10^{-5}	0
290	4.18×10^{-5}	7.7×10^{-5}	1.09×10^{-4}	0	-9.85×10^{-5}	0
320	6.54×10^{-5}	2.26×10^{-4}	9.08×10^{-5}	0	-2.26×10^{-4}	0

Table 3 Temperature dependence of the eigenvalues of the thermal expansion for **Bpe-BPh$_4$**

Temp.[K]	α_1	α_2	α_3
140	-4.01×10^{-5}	9.87×10^{-5}	1.71×10^{-4}
170	-4.32×10^{-5}	4.97×10^{-5}	1.02×10^{-4}
200	-2.29×10^{-5}	8.27×10^{-5}	1.21×10^{-4}
230	-3.94×10^{-5}	9.92×10^{-5}	1.49×10^{-4}
260	-2.62×10^{-5}	7.87×10^{-5}	1.56×10^{-4}
290	-2.88×10^{-5}	7.70×10^{-5}	1.79×10^{-4}
320	-1.48×10^{-4}	2.26×10^{-4}	3.05×10^{-4}

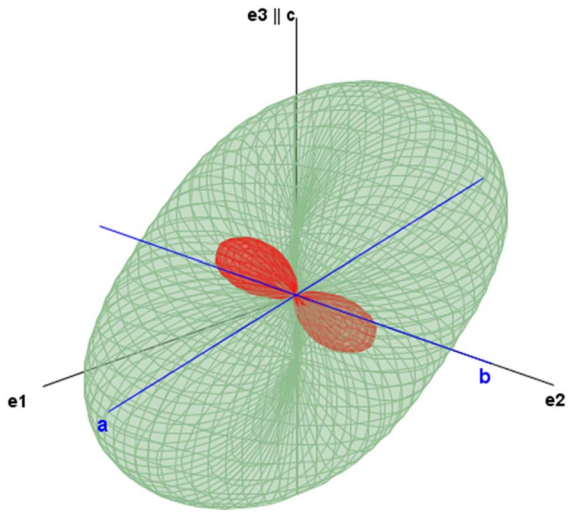

Fig. 4 Representation surface of the thermal expansion tensor for **Bpe-BPh$_4$** at 320 K. (Red parts of the surface indicate directions with negative values of thermal expansion).

Theoretical calculations and structural analyses consistently demonstrate that thermal expansion along the *c*-axis dominates the anisotropic behaviour of the material. This phenomenon is intrinsically related to the structural characteristics of the compound. As shown in Fig. S1 and S2, HBpe$^+$ molecules form one-dimensional hydrogen-bonded chains along the *c*-axis, where the flexibility of the hydrogen-bond network, coupled with the pedal motion of HBpe$^+$ drives significant thermal expansion. Although the percentage changes in unit cell parameters appear comparable across axes, the absolute expansion along the *c*-axis (0.33 Å) actually exceeds that of the *a*-axis (0.17 Å) and *b*-axis (0.16 Å) due to its greater initial length. The thermal expansion tensor analysis (Tables 2, 3 and Fig. 4) further confirms this conclusion, revealing that the principal expansion eigenvalue ($\alpha_3 = 3.05 \times 10^{-4}$ K^{-1} at 320 K) aligns with the *c*-axis direction and serves as the dominant contributor to the overall volume expansion. Additionally, the presence of the BPh_4^- component plays a crucial role in stabilizing the structure. By providing a rigid framework, BPh_4^- helps balance the charge distribution and enhances the overall stability of the crystal lattice.

Conclusions

In this work, an organic co-crystal, named **Bpe-BPh$_4$**, containing 1,2-bis(4-pyridyl)-ethylene (Bpe), has been successfully obtained, in which the protonated HBpe$^+$ moieties serve as primary linkers to form one-dimensional chains through intermolecular hydrogen bonding. The resulting hydrogen-bonded supramolecular assembly exhibits pronounced temperature-dependent behaviour, providing a model system for dynamic materials and a versatile platform for multi-dimensionally functional assemblies. Noteworthily, the HBpe$^+$ molecules in **Bpe-BPh$_4$** behave as a dynamic pedal motion with rotation and vibration, thereby exhibiting an interesting TE behaviour. The variable-temperature SCXRD measurements further reveal the temperature-dependent disorder and the molecular motion of HBpe$^+$ groups in the co-crystal, and thus providing us with a significant perspective on the dynamic processes in ionic co-crystals.

Conflicts of interest

There are no conflicts to declare.

Data availability

The data that support the findings of this study are available from the corresponding author upon reasonable request.

CCDC 2412181–2412187 contain the supplementary crystallographic data for this paper.[21a–g]

Supplementary information: experimental procedures and protocols. See DOI: https://doi.org/10.1039/d5ra04941e.

Acknowledgements

This work was supported by the NSFC (22463010, 22063008 and 22406098), the Project of Central Government Guides Local

Science and Technology Development (2024FRD05053), the Natural Science Foundation of Ningxia Province (2023AAC03227, 2024BEH04153 and 2023AAC03014), the Young Top-notch Talent Cultivation Program of Ningxia Province, and the Discipline Project of Ningxia (NXYLXK2017A04).

References

1 I. E. Claassens, L. J. Barbour and D. A. Haynes, *J. Am. Chem. Soc.*, 2019, **141**, 11425–11429.
2 C. A. Gunawardana and C. B. Aakeröy, *Chem. Commun.*, 2018, **54**, 14047–14060.
3 G. Campillo-Alvarado, C. Li, D. C. Swenson and L. R. MacGillivray, *Cryst. Growth Des.*, 2019, **19**, 2511–2518.
4 K. Lisac, F. Topić, M. Arhangelskis, S. Cepić, P. A. Julien, C. W. Nickels, A. J. Morris, T. Friščić and D. Cinčić, *Nat. Commun.*, 2019, **10**, 61.
5 Y.-G. Huang, Y. Shiota, S.-Q. Su, S.-Q. Wu, Z.-S. Yao, G.-L. Li, S. Kanegawa, S. Kang, T. Kamachi, K. Yoshizawa, K. Ariga and O. Sato, *Angew. Chem., Int. Ed.*, 2016, **55**, 14628–14632.
6 A. van der Lee and D. G. Dumitrescu, *Chem. Sci.*, 2021, **12**, 8537–8547.
7 Y. Wu, D. Tian, J. Ferrando-Soria, J. Cano, L. Yin, Z. Ouyang, Z. Wang, S. Luo, X. Liu and E. Pardo, *Inorg. Chem. Front.*, 2019, **6**, 848–856.
8 W. Zhu, R. Zheng, Y. Zhen, Z. Yu, H. Dong, H. Fu, Q. Shi and W. Hu, *J. Am. Chem. Soc.*, 2015, **137**, 11038–11046.
9 E. A. Sprague-Klein, B. Negru, L. R. Madison, S. C. Coste, B. K. Rugg, A. M. Felts, M. O. McAnally, M. Banik, V. A. Apkarian, M. R. Wasielewski, M. A. Ratner, T. Seideman, G. C. Schatz and R. P. Van Duyne, *J. Am. Chem. Soc.*, 2018, **140**, 10583–10592.
10 Y.-L. Xu, Q. Gao, M. Zhao, H.-J. Zhang, Y.-H. Zhang and Z. Chang, *Chin. Chem. Lett.*, 2017, **28**, 55–59.
11 J. Harada and K. Ogawa, *Chem. Soc. Rev.*, 2009, **38**, 2244–2252.
12 N. Juneja, D. K. Unruh, E. Bosch, R. H. Groeneman and K. M. Hutchins, *New J. Chem.*, 2019, **43**, 18433–18436.
13 H. Chi, Y. Liu, Z. Li, W. Chen and Y. He, *Nat. Commun.*, 2023, **14**, 5061.
14 K. M. Hutchins, D. K. Unruh, F. A. Verdu and R. H. Groeneman, *Cryst. Growth Des.*, 2018, **18**, 566–570.
15 A. Christy, *Acta Crystallogr., Sect. B*, 1995, **51**, 753–757.
16 N. Juneja, D. K. Unruh, G. C. George, III and K. M. Hutchins, *Cryst. Growth Des.*, 2023, **23**, 524–531.
17 S. Bhattacharya and B. K. Saha, *Cryst. Growth Des.*, 2012, **12**, 4716–4719.
18 K. M. Hutchins, R. H. Groeneman, E. W. Reinheimer, D. C. Swenson and L. R. MacGillivray, *Chem. Sci.*, 2015, **6**, 4717–4722.
19 G. Kresse and D. Joubert, *Phys. Rev. B: Condens. Matter Mater. Phys.*, 1999, **59**, 1758–1775.
20 T. Langreiter and V. Kahlenberg, *Crystals*, 2015, **5**, 143–153.
21 (*a*) Y. Zhang, Y. Jiao, Y. Guo, P. Cen, Z. Zhang and X. Liu, CCDC 2412181: Experimental Crystal Structure Determination, 2025, DOI: **10.5517/ccdc.csd.cc2lz29z**.; (*b*) Y. Zhang, Y. Jiao, Y. Guo, P. Cen, Z. Zhang and X. Liu, CCDC 2412182: Experimental Crystal Structure Determination, 2025, DOI: **10.5517/ccdc.csd.cc2lz2b0**; (*c*) Y. Zhang, Y. Jiao, Y. Guo, P. Cen, Z. Zhang and X. Liu, CCDC 2412183: Experimental Crystal Structure Determination, 2025, DOI: **10.5517/ccdc.csd.cc2lz2c1**; (*d*) Y. Zhang, Y. Jiao, Y. Guo, P. Cen, Z. Zhang and X. Liu, CCDC 2412184: Experimental Crystal Structure Determination, 2025, DOI: **10.5517/ccdc.csd.cc2lz2d2**; (*e*) Y. Zhang, Y. Jiao, Y. Guo, P. Cen, Z. Zhang and X. Liu, CCDC 2412185: Experimental Crystal Structure Determination, 2025, DOI: **10.5517/ccdc.csd.cc2lz2f3**; (*f*) Y. Zhang, Y. Jiao, Y. Guo, P. Cen, Z. Zhang and X. Liu, CCDC 2412186: Experimental Crystal Structure Determination, 2025, DOI: **10.5517/ccdc.csd.cc2lz2g4**; (*g*) Y. Zhang, Y. Jiao, Y. Guo, P. Cen, Z. Zhang and X. Liu, CCDC 2412187: Experimental Crystal Structure Determination, 2025, DOI: **10.5517/ccdc.csd.cc2lz2h5**.